Supplementary Materials

Materials and methods

Computational analysis

The RNA sequencing data and corresponding clinical information of 17 solid cancer types in TCGA (The Cancer Genome Atlas) were collected and processed as previously described[1]. The 17 solid cancer types include BLCA (bladder urothelial carcinoma), BRCA (breast invasive carcinoma), CESC (cervical & endocervical cancer), COAD (colon adenocarcinoma), HNSC (head & neck squamous cell carcinoma), KICH (kidney chromophobe), KIRC (kidney clear cell carcinoma), KIRP (kidney papillary cell carcinoma), LIHC (liver hepatocellular carcinoma), LUAD (lung adenocarcinoma), LUSC (lung squamous cell carcinoma), OV (ovarian serous cystadenocarcinoma), PRAD (prostate adenocarcinoma), SKCM (skin cutaneous melanoma), STAD (stomach adenocarcinoma), THCA (thyroid carcinoma), and UCEC (uterine corpus endometrioid carcinoma)[2]. The RNA sequencing data and corresponding clinical information of the remaining 16 cancer types were also collected for validation. The remaining 16 cancer types include ACC (adrenocortical cancer), CHOL (cholangiocarcinoma), DLBC (diffuse large B-cell lymphoma), ESCA (esophageal carcinoma), GBM (glioblastoma multiforme), HNSC (head & neck squamous cell carcinoma), LAML (acute myeloid leukemia), LGG (brain lower grade glioma), MESO (mesothelioma), PAAD (pancreatic adenocarcinoma), PCPG (pheochromocytoma & paraganglioma), READ (rectum adenocarcinoma), SARC (sarcoma), TGCT (testicular germ cell tumor), THYM (thymoma), UCS (uterine carcinosarcoma), UVM (uveal melanoma). And the corresponding data of normal tissues were obtained from GTEx (Genotype-Tissue Expression)[3]. TRPM family members were collected from a previous study[4]. The mutation frequency (truncating and missense) scores and somatic copy number alteration (SCNA) (amplification and deep deletion) were calculated. Values of the SCNA scores equal to 2 and -2 were referred to as amplification and deep deletion, respectively[5]. Each TRPM family member was paired with the rest prognostically notable genes to form gene pairs. Ea was regarded as the expression value of Gene a, and similarly, Eb represented the expression values of Gene b. The corresponding

GenePair(ab) value was calculated based on their relative expression values:

$$GenePair(ab) = \begin{cases} 1, & Ea > Eb \\ 0, & Ea < Eb \end{cases}$$

Then C-index analysis of GenePair(ab) was performed, and GenePair(ab) was selected as a prognostic risk factor with the largest C-index. The eight TRP-based gene pairs are TRPM1_VS_SLC5A8, TRPM2_VS_ENPP5, CYP2C18_VS_TRPM3, UBE2C_VS_TRPM4, TRPM5_VS_PCAT18, CYP2C18_VS_TRPM, ANLN_VS_TRPM7, and CASC9_VS_TRPM8. Survival analysis was performed on the gene pair-related groups (0 and 1). A least absolute shrinkage and selection operator regularized Cox regression (LassoCox)-based TRPM-Score was calculated based on the eight most potent gene pairs as follows: 0.235*TRPM1_VS_SLC5A8 + 0.1107*TRPM2_VS_ENPP5 + 0.0917*CYP2C18_VS_TRPM3 + 0.6346*UBE2C_VS_TRPM4 + 0.1936*TRPM5_VS_PCAT18 + 0.3083*CYP2C18_VS_TRPM6 + 0.2081*ANLN_VS_TRPM7 + 0.1399*CASC9_VS_TRPM8.

The differentially expressed genes (DEGs) between two TRPM-Score groups were identified using the R package limma[6]. Six machine learning algorithms for classification were used to screen the most potent DEGs, including Random Forest[7], support vector machine (SVM)[8], prediction analysis for microarrays (Pamr)[9], XGBoost[10], Boruta[11], and least absolute shrinkage and selection operator regularized logistic regression (LassoLR)[12, 13]. Another six machine learning algorithms for survival, CoxBoost[14], StepwiseCox Forward, StepwiseCox Both, StepwiseCox Backward, Random Survival Forest[15], and LassoCox[16], were applied to further determine the most prognostic DEGs[17]. A deep learning algorithm, Autoencoder, was used to determine the most valuable DEG, CCNE1[18]. A univariate Cox proportional hazards regression analysis was performed on TRPM-Score and CCNE1 to assess their prognostic value in pan-cancer. Tumor Mutational Burden (TMB), Microsatellite Instability (MSI), Cytolytic Activity (CYT), and T Cell-Inflamed Signature (GEP) were collected as previously described[19]. Stromal Score, Immune Score, ESTIMATE Score, and Tumor Purity generated by Estimation of STromal and

Immune cells in MAlignant Tumor tissues using Expression data (ESTIMATE) have been collected[20]. Gene set enrichment analysis (GSEA) was performed on TRPM-Score and CCNE1 to explore their immune functions[21]. Gene Ontology (GO)[22] and Kyoto Encyclopedia of Genes and Genomes (KEGG)[23] enrichment analysis were performed. Data for immune checkpoint blockade (ICB) therapy of SKCM were sourced from ICBatlas[24] and ICBnetIS[25]. The SKCM ICB samples were collected from 10 published patient cohorts: Abril-Rodriguez[26], Amato[27], Auslander[28], Freeman[29], Gide[30], Hugo[31], Liu[32], Riaz[33], Van-Allen[34], and Zappasodi[35]. Other five SKCM datasets with survival information namely GSE19234[36], GSE22155[37], GSE53118[38], GSE65904[39], and GSE98364[40] were obtained from GEO (Gene Expression Omnibus). Other immunotherapy cohorts, including NSCLC data from Cho[41] and Jung[42], STAD data from Kim[43], LIHC data from Hong[44], GBM data from Zhao[45], and KIRC data from Miao[46] were also collected. Student's t-test and one-way analysis of variance (ANOVA) were used to compare normally distributed variables between the two groups and multiple groups, respectively. The Wilcoxon and Kruskal-Wallis tests were utilized to compare the non-normally distributed data between the two groups and multiple groups, respectively.

In vitro validation

The hepG2 (LIHC), MCF-7 (BRCA), SK-MEL-28 (SKCM), and THP-1 cell lines were purchased from iCell (https://www.icellbioscience.com). Three siRNA sequences (Sense CCGAGCAAAGAAAGCCAUGUUTT Antisense AACAUGGCUUUCUUUGCUCGGTT; Sense GCAAUUCUUCUGGAUUGGUUATT Antisense UAACCAAUCCAGAAGAAUUGCTT; Sense CCUUGUAUCAUUUCUCGUCAUTT Antisense AUGACGAGAAAUGAUACAAGGTT) were used to suppress the expression of CCNE1. CCNE1 (11554-1-AP, Rabbit, Proteintech), PD-L1 (66248-1-Ig, Mouse, Proteintech), and β-actin (66009-1-Ig, Mouse, Proteintech) were used as the primary antibodies in Western Blot assay. HRP goat anti-mouse IgG (SA00001-1, Proteintech) and HRP goat anti-rabbit IgG (SA00001-2, Proteintech) were used as the secondary

antibodies in Western Blot assay.

The hepG2 and MCF-7 cells were cultured in DMEM medium containing 10% FBS and 1% antibiotic-antimycotic, and the SK-MEL-28 cells were cultured in 1640 medium containing 10% FBS and 1% antibiotic-antimycotic. All the cell lines were cultured in a 37°C, 5% CO2, and humidified incubator.

The hepG2, MCF-7, and SK-MEL-28 cells were seeded in 6-well plates at a density of 1x10^5 cells per well. The cells were then transfected with si-NC and si-CCNE1 and cultured for 48 hours.

The THP-1 cells were centrifuged and resuspended in 1640 medium containing 320 nM of Phorbol 12-myristate 13-acetate (PMA). The cells were then seeded in a 6-well plate and incubated at 37°C for 6 hours, during which time the THP-1 cells transformed from suspension to adherent M0 cells. Simultaneously, the hepG2, MCF-7, SK-MEL-28, and M0 cells were detached using trypsin, centrifuged, and resuspended in their respective complete growth media. The hepG2, MCF-7, and SK-MEL-28 cells were then seeded in the lower chamber of a co-culture Transwell system with 8 μm pore size, and the M0 cells were added to the upper chamber of the Transwell. The co-culture was maintained for 48 hours. After the co-culture, the supernatant was removed, and the cells were washed with PBS, fixed with paraformaldehyde, and stained with crystal violet for imaging.

The human pan-cancer tissue array (MTU1021) was purchased from Wuhan Tanda Scientific Co., LTD company. CCNE1 (11554-1-AP, Proteintech), CD8 (66868-1-Ig, Proteintech), CD68 (GB113150, Serviebio), and CD163 (16646-1-AP, Proteintech) were used as the primary antibodies in multiplex immunofluorescence staining assay. HRP goat anti-mouse IgG (GB23301, Servicebio) and HRP goat anti-rabbit IgG (GB23303, Servicebio) were used as the secondary antibodies in multiplex immunofluorescence staining assay. After labeling with the human antigens, nuclei were stained with 4′,6-Diamidino2-phenylindole dihydrochloride (DAPI), and an antifade mounting medium was applied. Stained slides were scanned using the TissueFAXS platform (TissueGnostics, Vienna, Austria) at 10X magnification. The scans were combined to build a single stack image. Spectral libraries were established.

Single-stained slides were applied to extract the spectrum of autofluorescence of tissues and each fluorescein, respectively. The library was then used to unmix the multispectral images with the StrataQuest software (TissueGnostics, Vienna, Austria). Regarding fluorescence spectra, DAPI glows blue, CY3 (CD68) glows red, CY5 (CD8) glows pink, FITC (CD163) glows green, and 594 (CCNE1) glows orange.

References

1. Wang G, Xu D, Zhang Z, Li X, Shi J, Sun J, Liu HZ, Li X, Zhou M, Zheng T: **The pan-cancer landscape of crosstalk between epithelial-mesenchymal transition and immune evasion relevant to prognosis and immunotherapy response.** *NPJ Precis Oncol* 2021, **5**:56.
2. Cancer Genome Atlas Research N, Weinstein JN, Collisson EA, Mills GB, Shaw KR, Ozenberger BA, Ellrott K, Shmulevich I, Sander C, Stuart JM: **The Cancer Genome Atlas Pan-Cancer analysis project.** *Nat Genet* 2013, **45**:1113-1120.
3. Lonsdale J, Thomas J, Salvatore M, Phillips R, Lo E, Shad S, Hasz R, Walters G, Garcia F, Young N, et al: **The Genotype-Tissue Expression (GTEx) project.** *Nature Genetics* 2013, **45**:580-585.
4. Samanta A, Hughes TET, Moiseenkova-Bell VY: **Transient Receptor Potential (TRP) Channels.** *Subcell Biochem* 2018, **87**:141-165.
5. Knijnenburg TA, Wang L, Zimmermann MT, Chambwe N, Gao GF, Cherniack AD, Fan H, Shen H, Way GP, Greene CS, et al: **Genomic and Molecular Landscape of DNA Damage Repair Deficiency across The Cancer Genome Atlas.** *Cell Rep* 2018, **23**:239-254 e236.
6. Ritchie ME, Phipson B, Wu D, Hu Y, Law CW, Shi W, Smyth GK: **limma powers differential expression analyses for RNA-sequencing and microarray studies.** *Nucleic Acids Res* 2015, **43**:e47.
7. Petralia F, Wang P, Yang J, Tu Z: **Integrative random forest for gene regulatory network inference.** *Bioinformatics* 2015, **31**:i197-205.
8. Van Belle V, Van Calster B, Van Huffel S, Suykens JA, Lisboa P: **Explaining Support Vector Machines: A Color Based Nomogram.** *PLoS One* 2016, **11**:e0164568.
9. Tibshirani R, Hastie T, Narasimhan B, Chu G: **Diagnosis of multiple cancer types by shrunken centroids of gene expression.** *Proc Natl Acad Sci U S A* 2002, **99**:6567-6572.
10. López V, Fernández A, García S, Palade V, Herrera F: **An insight into classification with imbalanced data: Empirical results and current trends on using data intrinsic characteristics.** *Information Sciences* 2013, **250**:113-141.
11. Kursa MB, Jankowski A, Rudnicki WR: **Boruta - A System for Feature Selection.** *Fundamenta Informaticae* 2010, **101**:271-285.
12. Van Calster B, van Smeden M, De Cock B, Steyerberg EW: **Regression**

shrinkage methods for clinical prediction models do not guarantee improved performance: Simulation study. *Stat Methods Med Res* 2020, **29**:3166-3178.

13. Archer KJ, Williams AA: **L1 penalized continuation ratio models for ordinal response prediction using high-dimensional datasets.** *Stat Med* 2012, **31**:1464-1474.
14. De Bin R: **Boosting in Cox regression: a comparison between the likelihood-based and the model-based approaches with focus on the R-packages CoxBoost and mboost.** *Computational Statistics* 2016, **31**:513-531.
15. Ishwaran H, Kogalur UB, Blackstone EH, Lauer MS: **Random survival forests.** *The Annals of Applied Statistics* 2008, **2**.
16. Fan F, Zhang H, Dai Z, Zhang Y, Xia Z, Cao H, Yang K, Hu S, Guo Y, Ding F, et al: **A comprehensive prognostic signature for glioblastoma patients based on transcriptomics and single cell sequencing.** *Cell Oncol (Dordr)* 2021, **44**:917-935.
17. Zhang N, Zhang H, Liu Z, Dai Z, Wu W, Zhou R, Li S, Wang Z, Liang X, Wen J, et al: **An artificial intelligence network-guided signature for predicting outcome and immunotherapy response in lung adenocarcinoma patients based on 26 machine learning algorithms.** *Cell Prolif* 2023, **56**:e13409.
18. Zhang Z, Chen H, Yan D, Chen L, Sun J, Zhou M: **Deep learning identifies a T-cell exhaustion-dependent transcriptional signature for predicting clinical outcomes and response to immune checkpoint blockade.** *Oncogenesis* 2023, **12**:37.
19. Zhang H, Wang Z, Dai Z, Wu W, Cao H, Li S, Zhang N, Cheng Q: **Novel Immune Infiltrating Cell Signature Based on Cell Pair Algorithm Is a Prognostic Marker in Cancer.** *Front Immunol* 2021, **12**:694490.
20. Yoshihara K, Shahmoradgoli M, Martí nez E, Vegesna R, Kim H, Torres-Garcia W, Treviño V, Shen H, Laird PW, Levine DA, et al: **Inferring tumour purity and stromal and immune cell admixture from expression data.** *Nature Communications* 2013, **4**.
21. Subramanian A, Tamayo P, Mootha VK, Mukherjee S, Ebert BL, Gillette MA, Paulovich A, Pomeroy SL, Golub TR, Lander ES, Mesirov JP: **Gene set enrichment analysis: a knowledge-based approach for interpreting genome-wide expression profiles.** *Proc Natl Acad Sci U S A* 2005, **102**:15545-15550.
22. Gene Ontology C: **Gene Ontology Consortium: going forward.** *Nucleic Acids Res* 2015, **43**:D1049-1056.
23. Kanehisa M, Furumichi M, Sato Y, Ishiguro-Watanabe M, Tanabe M: **KEGG: integrating viruses and cellular organisms.** *Nucleic Acids Res* 2021, **49**:D545-D551.
24. Yang M, Miao YR, Xie GY, Luo M, Hu H, Kwok HF, Feng J, Guo AY: **ICBatlas: A Comprehensive Resource for Depicting Immune Checkpoint Blockade Therapy Characteristics from Transcriptome Profiles.** *Cancer Immunol Res* 2022, **10**:1398-1406.

25. Zhang N, Yang M, Yang JM, Zhang CY, Guo AY: **A Predictive Network-Based Immune Checkpoint Blockade Immunotherapeutic Signature Optimizing Patient Selection and Treatment Strategies.** *Small Methods* 2024, **8**:e2301685.
26. Abril-Rodriguez G, Torrejon DY, Liu W, Zaretsky JM, Nowicki TS, Tsoi J, Puig-Saus C, Baselga-Carretero I, Medina E, Quist MJ, et al: **PAK4 inhibition improves PD-1 blockade immunotherapy.** *Nat Cancer* 2020, **1**:46-58.
27. Amato CM, Hintzsche JD, Wells K, Applegate A, Gorden NT, Vorwald VM, Tobin RP, Nassar K, Shellman YG, Kim J, et al: **Pre-Treatment Mutational and Transcriptomic Landscape of Responding Metastatic Melanoma Patients to Anti-PD1 Immunotherapy.** *Cancers (Basel)* 2020, **12**.
28. Auslander N, Zhang G, Lee JS, Frederick DT, Miao B, Moll T, Tian T, Wei Z, Madan S, Sullivan RJ, et al: **Robust prediction of response to immune checkpoint blockade therapy in metastatic melanoma.** *Nat Med* 2018, **24**:1545-1549.
29. Freeman SS, Sade-Feldman M, Kim J, Stewart C, Gonye ALK, Ravi A, Arniella MB, Gushterova I, LaSalle TJ, Blaum EM, et al: **Combined tumor and immune signals from genomes or transcriptomes predict outcomes of checkpoint inhibition in melanoma.** *Cell Rep Med* 2022, **3**:100500.
30. Gide TN, Quek C, Menzies AM, Tasker AT, Shang P, Holst J, Madore J, Lim SY, Velickovic R, Wongchenko M, et al: **Distinct Immune Cell Populations Define Response to Anti-PD-1 Monotherapy and Anti-PD-1/Anti-CTLA-4 Combined Therapy.** *Cancer Cell* 2019, **35**:238-255 e236.
31. Hugo W, Zaretsky JM, Sun L, Song C, Moreno BH, Hu-Lieskovan S, Berent-Maoz B, Pang J, Chmielowski B, Cherry G, et al: **Genomic and Transcriptomic Features of Response to Anti-PD-1 Therapy in Metastatic Melanoma.** *Cell* 2017, **168**:542.
32. Liu D, Schilling B, Liu D, Sucker A, Livingstone E, Jerby-Arnon L, Zimmer L, Gutzmer R, Satzger I, Loquai C, et al: **Integrative molecular and clinical modeling of clinical outcomes to PD1 blockade in patients with metastatic melanoma.** *Nat Med* 2019, **25**:1916-1927.
33. Riaz N, Havel JJ, Makarov V, Desrichard A, Urba WJ, Sims JS, Hodi FS, Martin-Algarra S, Mandal R, Sharfman WH, et al: **Tumor and Microenvironment Evolution during Immunotherapy with Nivolumab.** *Cell* 2017, **171**:934-949 e916.
34. Van Allen EM, Miao D, Schilling B, Shukla SA, Blank C, Zimmer L, Sucker A, Hillen U, Foppen MHG, Goldinger SM, et al: **Genomic correlates of response to CTLA-4 blockade in metastatic melanoma.** *Science* 2015, **350**:207-211.
35. Zappasodi R, Serganova I, Cohen IJ, Maeda M, Shindo M, Senbabaoglu Y, Watson MJ, Leftin A, Maniyar R, Verma S, et al: **CTLA-4 blockade drives loss of T(reg) stability in glycolysis-low tumours.** *Nature* 2021, **591**:652-658.
36. Bogunovic D, O'Neill DW, Belitskaya-Levy I, Vacic V, Yu YL, Adams S,

Darvishian F, Berman R, Shapiro R, Pavlick AC, et al: **Immune profile and mitotic index of metastatic melanoma lesions enhance clinical staging in predicting patient survival.** *Proc Natl Acad Sci U S A* 2009, **106:**20429-20434.

37. Kabbarah O, Nogueira C, Feng B, Nazarian RM, Bosenberg M, Wu M, Scott KL, Kwong LN, Xiao Y, Cordon-Cardo C, et al: **Integrative genome comparison of primary and metastatic melanomas.** *PLoS One* 2010, **5:**e10770.
38. Barter RL, Schramm SJ, Mann GJ, Yang YH: **Network-based biomarkers enhance classical approaches to prognostic gene expression signatures.** *BMC Syst Biol* 2014, **8 Suppl 4:**S5.
39. Cabrita R, Lauss M, Sanna A, Donia M, Skaarup Larsen M, Mitra S, Johansson I, Phung B, Harbst K, Vallon-Christersson J, et al: **Tertiary lymphoid structures improve immunotherapy and survival in melanoma.** *Nature* 2020, **577:**561-565.
40. Ono A, Sano O, Kazetani KI, Muraki T, Imamura K, Sumi H, Matsui J, Iwata H: **Feedback activation of AMPK-mediated autophagy acceleration is a key resistance mechanism against SCD1 inhibitor-induced cell growth inhibition.** *PLoS One* 2017, **12:**e0181243.
41. Cho JW, Hong MH, Ha SJ, Kim YJ, Cho BC, Lee I, Kim HR: **Genome-wide identification of differentially methylated promoters and enhancers associated with response to anti-PD-1 therapy in non-small cell lung cancer.** *Exp Mol Med* 2020, **52:**1550-1563.
42. Jung H, Kim HS, Kim JY, Sun JM, Ahn JS, Ahn MJ, Park K, Esteller M, Lee SH, Choi JK: **DNA methylation loss promotes immune evasion of tumours with high mutation and copy number load.** *Nat Commun* 2019, **10:**4278.
43. Kim ST, Cristescu R, Bass AJ, Kim KM, Odegaard JI, Kim K, Liu XQ, Sher X, Jung H, Lee M, et al: **Comprehensive molecular characterization of clinical responses to PD-1 inhibition in metastatic gastric cancer.** *Nat Med* 2018, **24:**1449-1458.
44. Hong JY, Cho HJ, Sa JK, Liu X, Ha SY, Lee T, Kim H, Kang W, Sinn DH, Gwak GY, et al: **Hepatocellular carcinoma patients with high circulating cytotoxic T cells and intra-tumoral immune signature benefit from pembrolizumab: results from a single-arm phase 2 trial.** *Genome Med* 2022, **14:**1.
45. Zhao J, Chen AX, Gartrell RD, Silverman AM, Aparicio L, Chu T, Bordbar D, Shan D, Samanamud J, Mahajan A, et al: **Immune and genomic correlates of response to anti-PD-1 immunotherapy in glioblastoma.** *Nat Med* 2019, **25:**462-469.
46. Miao D, Margolis CA, Gao W, Voss MH, Li W, Martini DJ, Norton C, Bosse D, Wankowicz SM, Cullen D, et al: **Genomic correlates of response to immune checkpoint therapies in clear cell renal cell carcinoma.** *Science* 2018, **359:**801-806.

Supplementary Figures

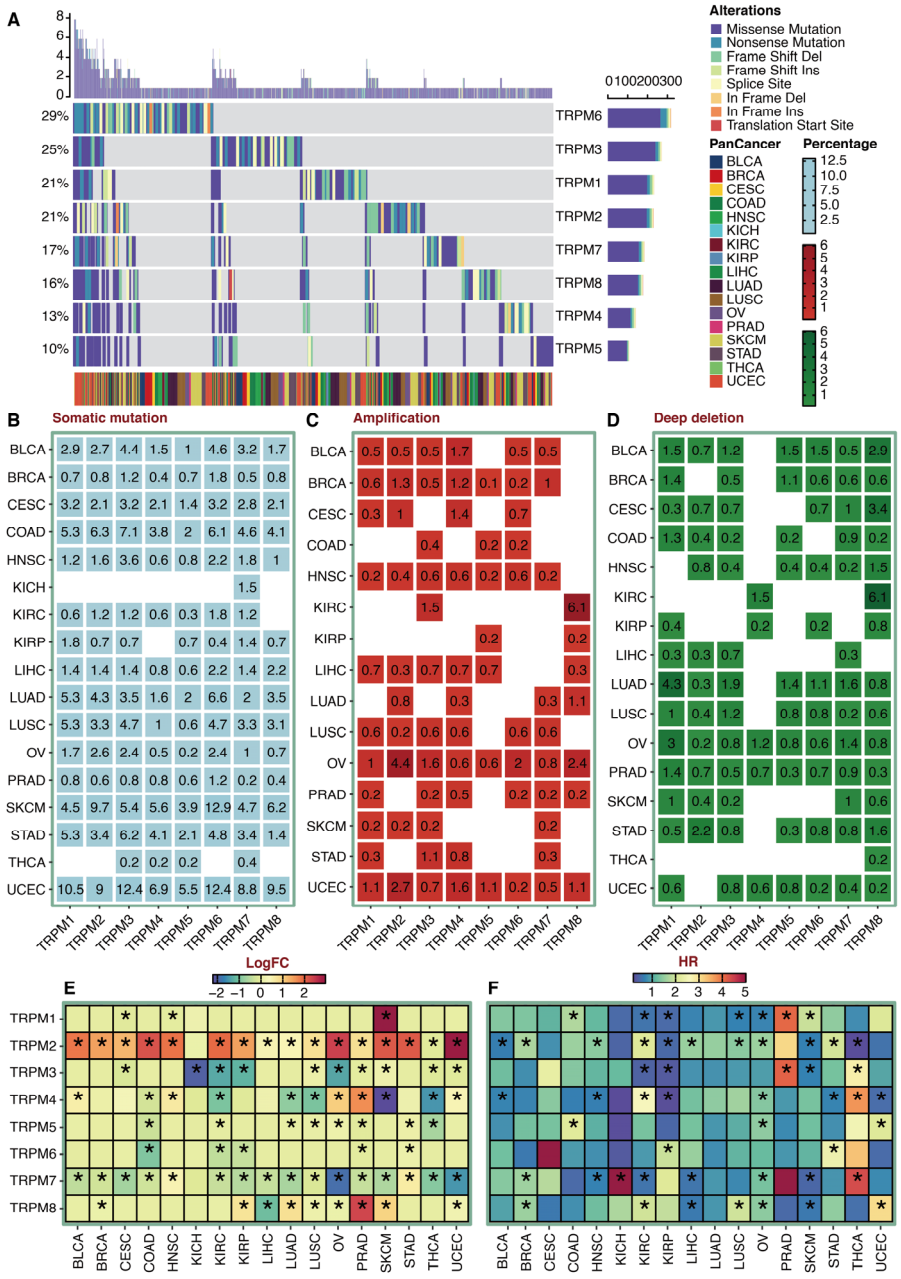

Figure S1. The mutation landscape and regulation network of TRPM family members.

A. Landscape of genomic alterations in the TRPM family members in pan-cancer. B. Distribution of mutation frequencies over cancer types. C. Distribution of amplification of SCNA frequencies over cancer types. D. Distribution of depletion of SCNA frequencies over cancer types. E. Differential expression analysis of TRPM family members in pan-cancer TCGA-based tumor tissues and GTEx-based normal tissues. F. Univariate Cox regression analysis on TRPM family members in pan-cancer.

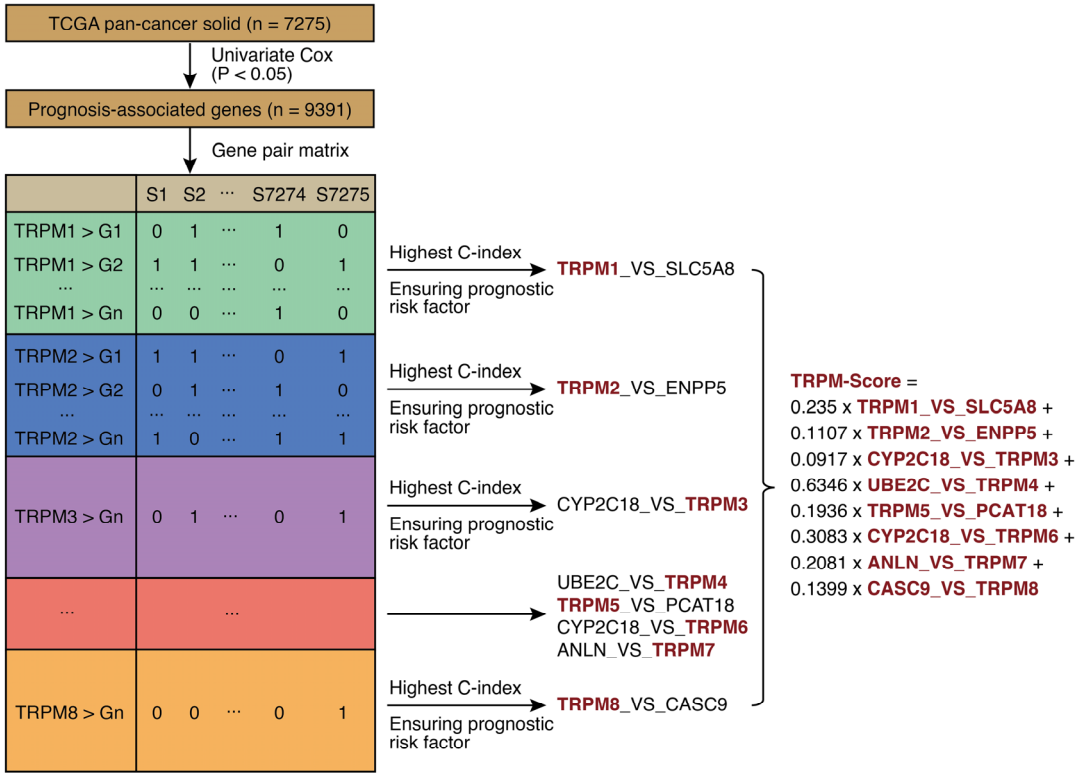

Figure S2. Flow diagram for the development of the TRPM-Score.

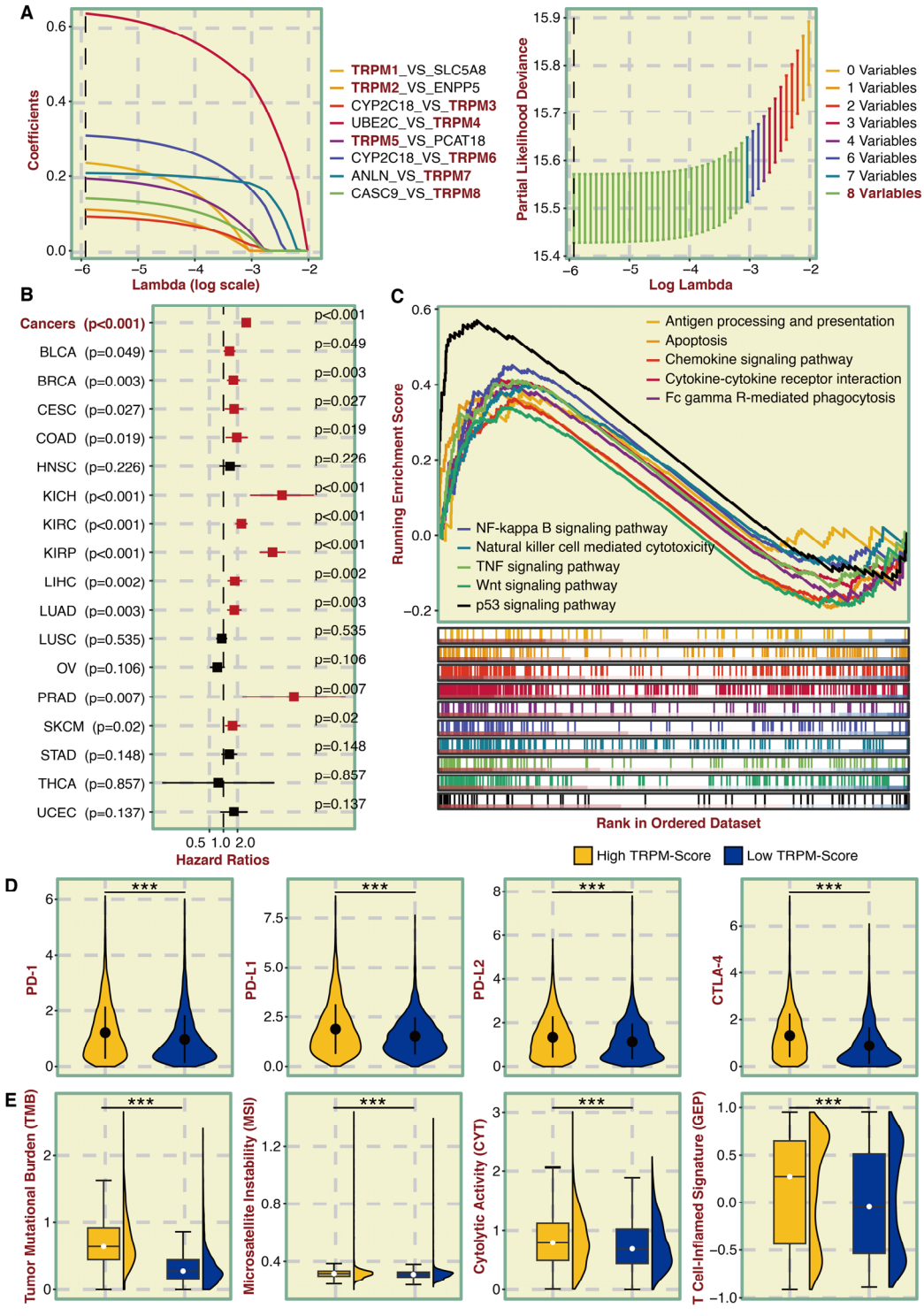

Figure S3. Predictive value and immunological features of the TRPM-Score.

A. Construction of LassoCox-based model to calculate the TRPM-Score. B. Univariate Cox regression analysis on TRPM-Score in pan-cancer. C. GSEA on TRPM-Score in pan-cancer. D. Violin plot showing the expression difference of PD-1, PD-L1, PD-L2, and CTLA-4 in TRPM-Score-based groups in pan-cancer. K. Violin plot showing TMB, CYT, MSI, and GEP levels in TRPM-Score-based groups in pan-cancer.

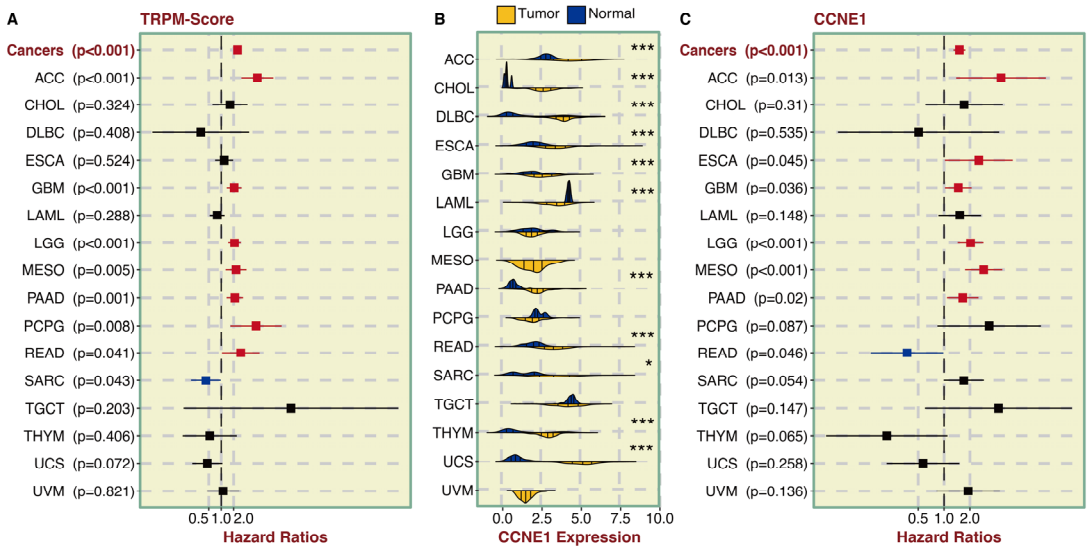

Figure S4. Investigation of TRPM-Score and CCNE1 across 16 additional cancer types.

A. Univariate Cox regression analysis of the TRPM-Score in the 16 additional cancer types. B. Violin plot showing the expression difference of CCNE1 in tumor and normal tissues in the 16 additional cancer types. C. Univariate Cox regression analysis of the TRPM-Score in the 16 additional cancer types.

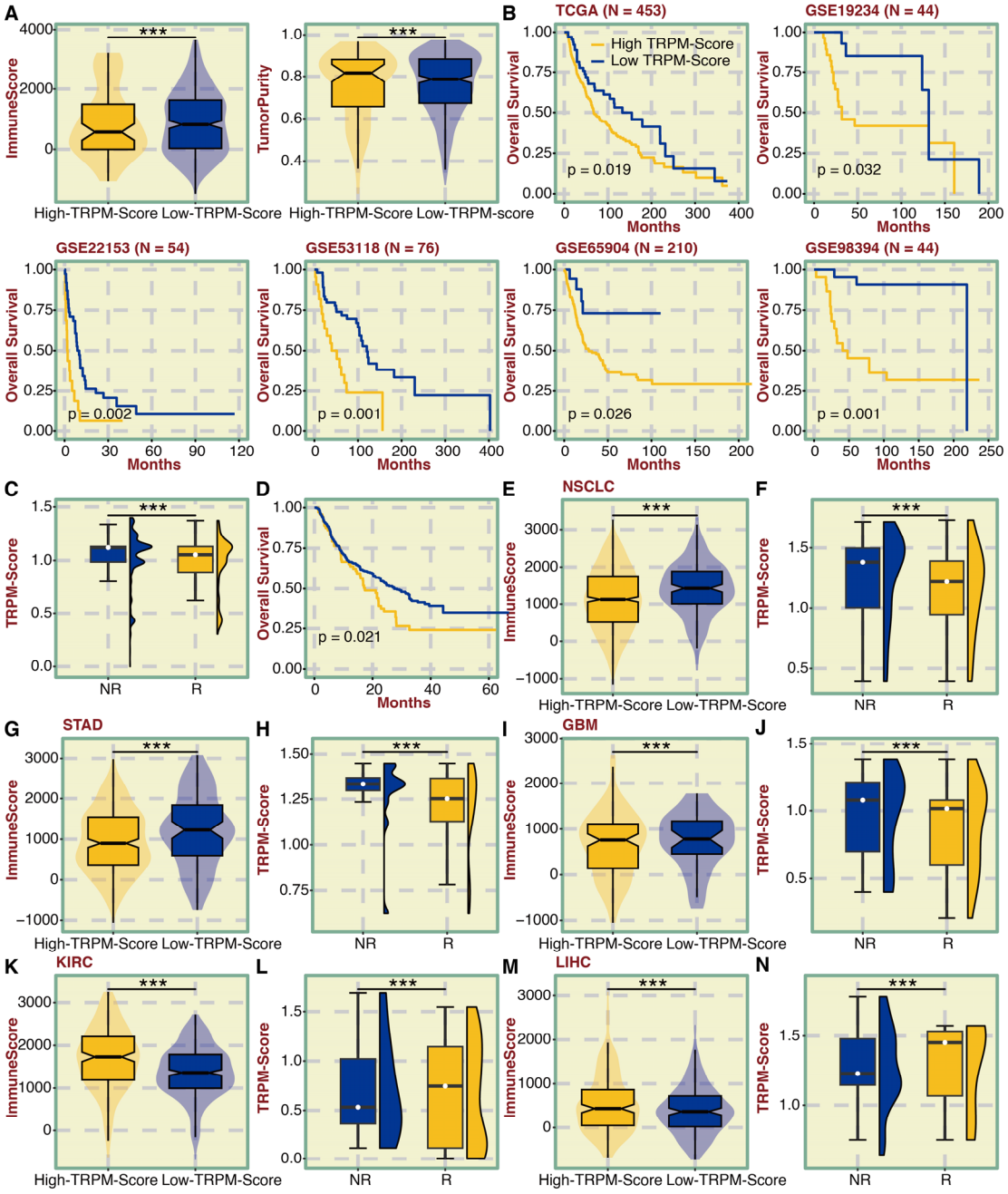

Figure S5. Predictive value of TRPM-Score for immunotherapy in cancer.

A. Box plot showing Immune Scores and Tumor Purity in the TRPM-Score-based groups in the TCGA-SKCM cohort. B. Survival curves of the TRPM-Score-based groups in the TCGA-SKCM cohort and additional cohorts: GSE19234, GSE22153, GSE53118, GSE65904, and GSE98394. C. Box plot showing TRPM-Scores in groups with different responses to ICB therapy in the SKCM ICB cohorts. D. Survival curves of the TRPM-Score-based groups in the SKCM ICB cohort. E. Box plot showing Immune Scores in the TRPM-Score-based groups in the TCGA-NSCLC cohort. F. Box

plot showing TRPM-Scores in groups with different responses to ICB therapy in the NSCLC ICB cohort. G. Box plot showing Immune Scores in the TRPM-Score-based groups in the TCGA-STAD cohort. H. Box plot showing TRPM-Scores in groups with different responses to ICB therapy in the STAD ICB cohorts. I. Box plot showing Immune Scores in the TRPM-Score-based groups in the TCGA-GBM cohort. J. Box plot showing TRPM-Scores in groups with different responses to ICB therapy in the GBM ICB cohorts. K. Box plot showing Immune Scores in the TRPM-Score-based groups in the TCGA-KIRC cohort. L. Box plot showing TRPM-Scores in groups with different responses to ICB therapy in the KIRC ICB cohort. M. Box plot showing Immune Scores in the TRPM-Score-based groups in the TCGA-LIHC cohort. N. Box plot showing TRPM-Scores in groups with different responses to ICB therapy in the LIHC ICB cohort.

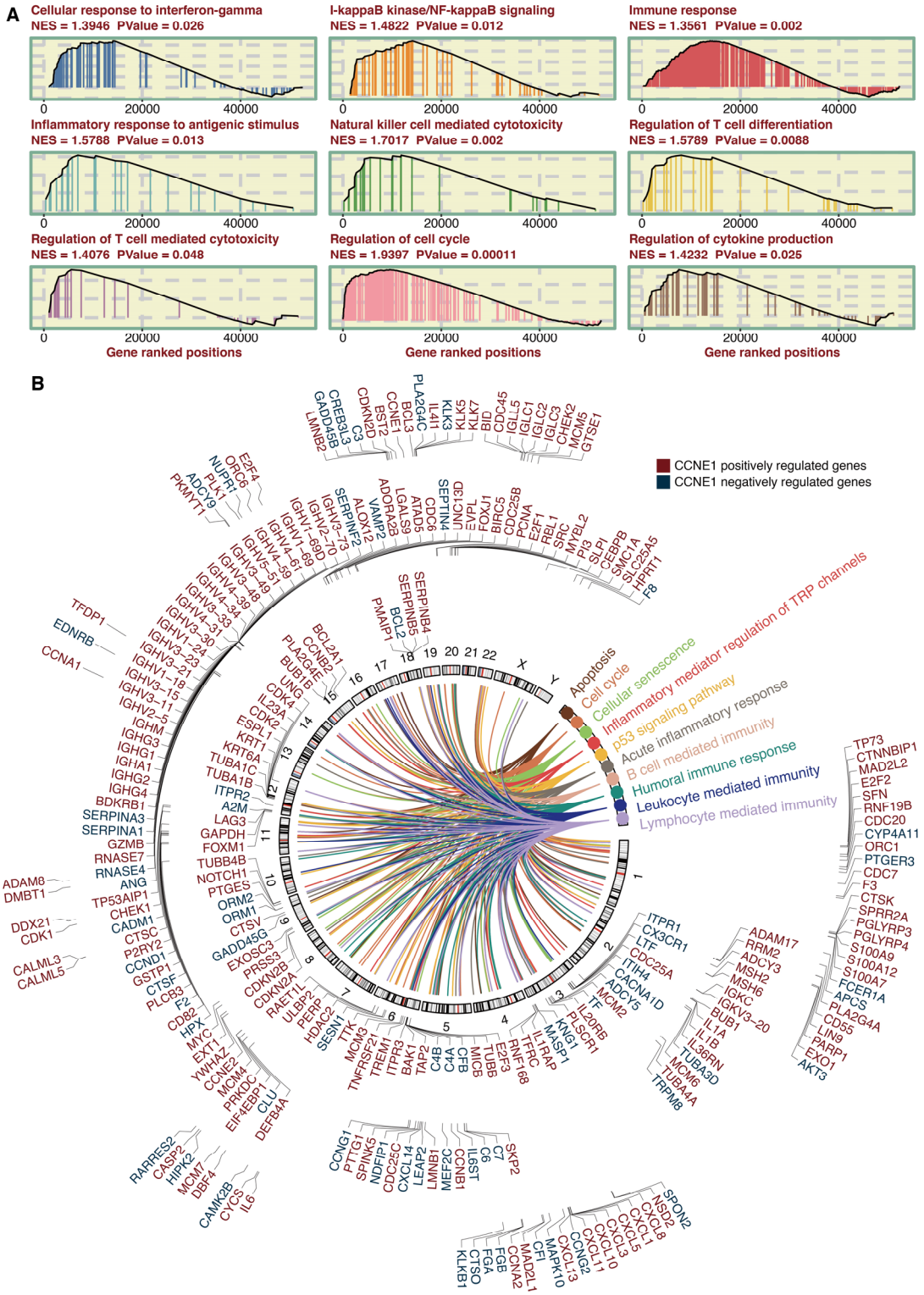

Figure S6. Functional annotation of CCNE1.

A. GSEA of GO pathways on CCNE1. B. GO and KEGG enrichment analysis on CCNE1. Pathway genes positively regulated by CCNE1 were labeled in red, and pathway genes negatively regulated by CCNE1 were labeled in blue.

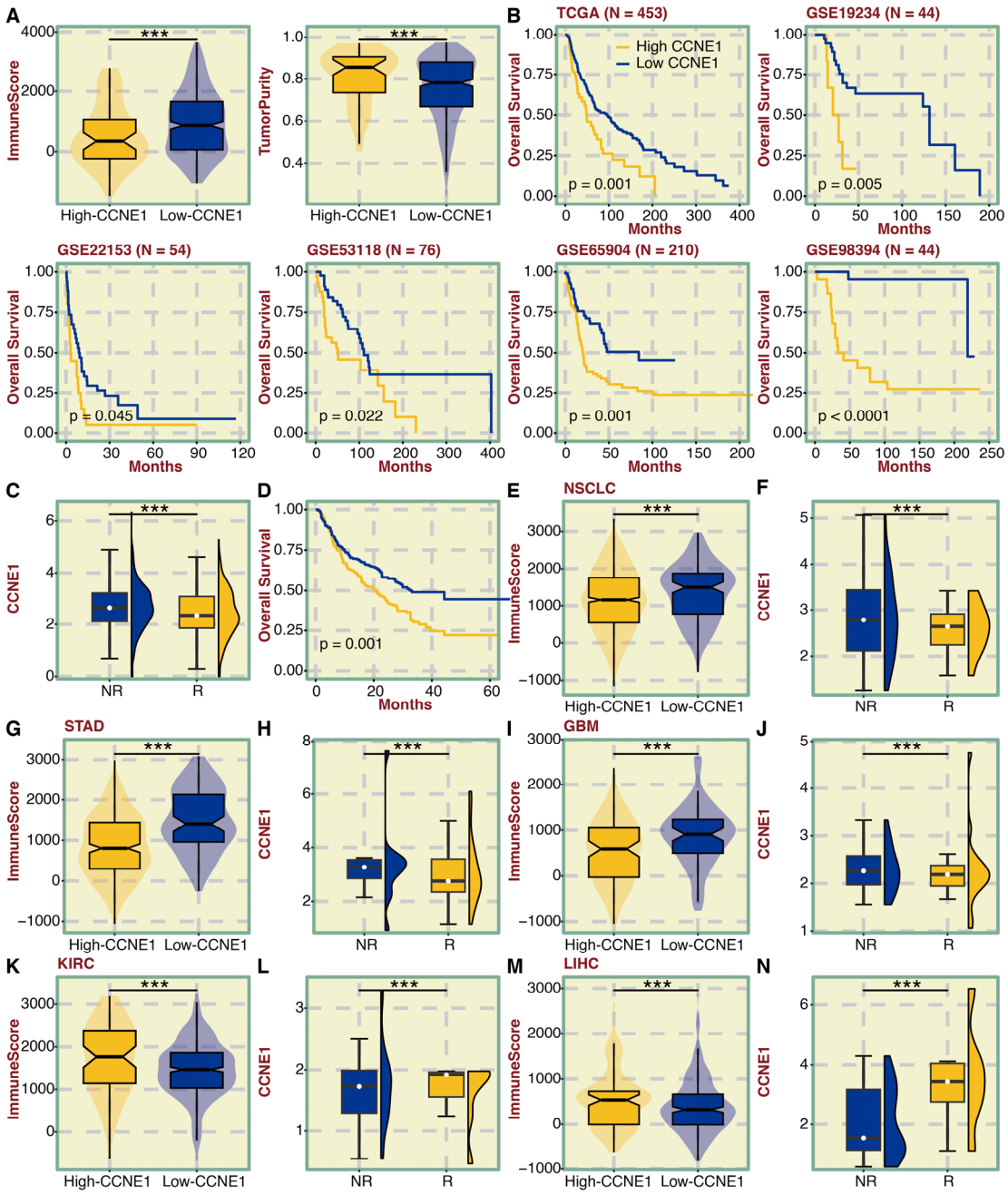

Figure S7. Predictive value of CCNE1 for immunotherapy in cancer.

A. Box plot showing Immune Scores and Tumor Purity in the CCNE1-based groups in the TCGA-SKCM cohort. B. Survival curves of the CCNE1-based groups in the TCGA-SKCM cohort and additional cohorts: GSE19234, GSE22153, GSE53118, GSE65904, and GSE98394. C. Box plot showing CCNE1 in groups with different responses to ICB therapy in the SKCM ICB cohorts. D. Survival curves of the CCNE1-based groups in the SKCM ICB cohort. E. Box plot showing Immune Scores in the CCNE1-based groups in the TCGA-NSCLC cohort. F. Box plot showing CCNE1 in

groups with different responses to ICB therapy in the NSCLC ICB cohort. G. Box plot showing Immune Scores in the CCNE1-based groups in the TCGA-STAD cohort. H. Box plot showing CCNE1 in groups with different responses to ICB therapy in the STAD ICB cohorts. I. Box plot showing Immune Scores in the CCNE1-based groups in the TCGA-GBM cohort. J. Box plot showing CCNE1 in groups with different responses to ICB therapy in the GBM ICB cohorts. K. Box plot showing Immune Scores in the CCNE1-based groups in the TCGA-KIRC cohort. L. Box plot showing CCNE1 in groups with different responses to ICB therapy in the KIRC ICB cohort. M. Box plot showing Immune Scores in the CCNE1-based groups in the TCGA-LIHC cohort. N. Box plot showing CCNE1 in groups with different responses to ICB therapy in the LIHC ICB cohort.